Decentralized Deconfliction Algorithms for Unicycle UAVs

Prachya Panyakeow and Mehran Mesbahi†

***Abstract*— This paper provides an approach for the collision avoidance problem for a group of unmanned aerial vehicles (UAV) modeled as unicycles. We use a combination of navigation and swirling functions to direct the vehicles along the planned trajectories while avoiding inter-vehicle collisions. The main contribution is to propose deconfliction algorithms for unicycle vehicles that more closely capture the dynamics of constant speed UAVs as opposed to double integrator models. Moreover, we consider the issue of aircraft turn-rate constraints and proceed to explore the selection of key algorithmic parameters in order to minimize undesirable trajectories and overshoot induced by the avoidance algorithm. The avoidance and convergence analysis of the proposed algorithm is performed for two UAV deconfliction and simulation results are provided to support the viability of the proposed framework for more general mission scenarios.**

I. Introduction

Collision avoidance has been a topic of great interest for multi-vehicle autonomous systems for several years. Modern technology allows groups of unmanned aerial vehicles (UAVs) to perform many civilian and military missions, including surveillance, monitoring, and reconnaissance. The conflict resolution becomes important when such missions require that UAVs operate in close proximity of each other. There has been a number of research works with various approaches to address conflict and collision avoidance between UAVs; see [10] for a survey. For example, in [11], the authors propose a set of prespecified maneuvers for each vehicle when a conflict is detected. On the other hand, optimization-based schemes, such as those discussed in [2], revolve around solving an optimization problem, often in a centralized way.

More closer to the present paper are approaches built around navigation functions. A navigation function landscapes the configuration space of the vehicles such that the goal points for the vehicles can be reached by following the function's descent direction. In [3] this idea was adopted for holonomic robots. Rimon and Koditschek [4] on the other hand, introduced a navigation function for robot obstacle avoidance in a generalized star world with a static environment along with the convergence analysis. Recently, the use of *decentralized navigation function* has gained attention in the area of cooperative and formation control of multiple agents. Being decentralized implies that each agent does not require knowledge of the desired destinations of other vehicles and only relies on limited information, such as relative position/velocity, from the "neighboring" agents. This reduces the computational aspects of gradient computation and communication and sensing requirements. Dimarogonas and Kyriakopoulos [13], [14] have utilized decentralized navigation functions for addressing collision avoidance between multiple *holonomic agents* in the absence of control constraints. In this paper, we use navigation functions, those which combine path planning and obstacle avoidance, to generate the required control input to the vehicles. More specifically, we focus on the use of *unicycle models* with turn-rate constraints in order to more accurately capture the non-holonomic dynamics of UAVs with constant speed. The algorithm presented here is an extension of [6], where the so-called "swirling effect" is introduced on a double integrator model to avoid stagnation points around the obstacles.

The contribution of this paper is twofold. On one hand, we examine the vehicles' turn-rates, trajectories overshoots, and minimum distance between the vehicles during the deconfliction. Moreover, we demonstrate how the algorithmic parameters can be chosen such that the vehicle actuator commands do not exceed prescribed limits without sacrificing performance. Additionally, the collision avoidance and the convergence of the algorithm are analyzed for a limited scenario and then verified for more general cases via simulations.

II. Problem Formulation

We consider a group of n homogeneous vehicles represented by non-holonomic unicycle model

$$\dot{x}_i(t) = U\cos\psi_i(t),\ \dot{y}_i(t) = U\sin\psi_i(t), \dot{\psi}_i(t) = u_i(t),$$

for $i = 1, ..., n$, where (x_i, y_i) specify the location of vehicle i measured relative to the earth frame. Every UAV is assumed to fly at a constant speed U. Moreover, the heading angle defines the orientation $\psi_i \in [-\pi, \pi]$ and its rate defines the input u_i. The constraints on turn-rates are imposed in the form of maximum limit

$$-\dot{\psi}_{max} \leq u_i(t) \leq \dot{\psi}_{max}. \tag{1}$$

We assume that each UAV has its nominal trajectory specified by a sequence of way-points. We incorporate the minimum turn radius to allow a smooth transition between the way-points. The way-point steering method is explained in [7]. Additionally, we use navigation functions to determine the desired headings for UAVs when a "conflict" is detected. Since the navigation function reflects the desire to follow the *nominal trajectory* while avoiding collisions, we refer to the algorithm as *deconfliction* as opposed to collision avoidance.

†P. Panyakeow and M. Mesbahi are with the Department of Aeronautics and Astronautics, University of Washington, Seattle, WA. Emails: *prachya@aa.washington.edu* and *mesbahi@aa.washington.edu*

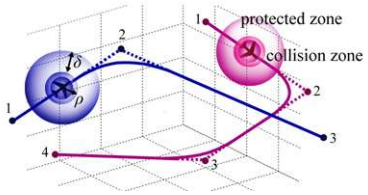

Fig. 1. Trajectories of UAVs

A conflict between two vehicles is defined by two virtual spheres in Fig. 1: collision zones of radius ρ and protected zone of radius $\rho + \delta$.

Definition 2.1: A *collision* between vehicle i and j occurs when their collision zones intersect or $\|\mathbf{r_{ij}}\| < \rho_i + \rho_j$, where $\mathbf{r_{ij}}$ is a vector from vehicle i and j.

Definition 2.2: Two vehicles i and j are in a *conflict* or *loss of separation* if their protected zones overlap, i.e., when $\|\mathbf{r_{ij}}\| < \rho_i + \rho_j + \delta_i + \delta_j$.

As it will be assumed that vehicle i can detect other vehicles within the range r_{ss}, we define the *neighborhood set* as

$$\mathcal{N}_i \triangleq \{j \neq i : \|\mathbf{r_{ij}}\| \leq r_{ss}\}. \tag{2}$$

Note that this set depends on the distances between vehicles, that is, it is a dynamic set. The goal of the control design is to specify the input u_i within the limit (1) such that all vehicles track their nominal trajectories as closely as possible while avoiding collisions or entering other vehicles' protected zones.

III. UAV Deconfliction

The deconfliction algorithm is built around a navigation function that utilizes the location of other vehicles in the set $\mathcal{N}_i$ as well as its nominal trajectory. Navigation functions are developed from the intuition that the trajectory of a dynamical system asymptotically approaches a state of minimum potential if it follows the descent direction of the potential. In this paper, the navigation function of each UAV is a mapping from a *free configuration space* $\mathcal{F}_i$, a region that the UAV is allowed to navigate in, to a potential value, as

$$V_i : \mathcal{F}_i \rightarrow \mathbf{R}. \tag{3}$$

Our free configuration space is a sphere representing the original space $\mathcal{C}_i$, with missing spheres representing other vehicles in $\mathcal{N}_i$, $\mathcal{O}_{ij}$; this will be denoted by $\mathcal{F}_i := \mathcal{C}_i \backslash \bigcup_{j \in \mathcal{N}_i} \mathcal{O}_{ij}$.

Let $\mathbf{q}_i = [x_i, y_i]^T$ represent the position state of vehicle i; $\mathbf{q}$ on the other hand, will denote the position state for all vehicles. The goal is to steer the group of UAVs from its initial state $\mathbf{q}_o$ to the destination $\mathbf{q}_d$ while avoiding the region $\mathcal{O}_{ij}$. The main idea behind the navigation function approach is to drive the UAVs using the negative gradient of the potential function by setting the desired velocity as

$$\mathbf{v}_i^d(t) = -\nabla_{\mathbf{q}_i} V_i(\mathbf{q}), \tag{4}$$

with the desire of leading the UAVs to a state with minimum potential value. Hence, it is desirable that the navigation function have a unique minimum at a destination state $\mathbf{q}_d$ and a maximum at the boundary of $\mathcal{F}$. However, other properties are also required to guarantee the desirable trajectories for the UAVs.

Definition 3.1: ([4]) Let $\mathcal{F}$ be the free configuration space and $q_d \in \mathcal{F}$ be the goal point of the UAV. A map $V : \mathcal{F} \rightarrow \mathbf{R}$ is a navigation function for the UAVs if it is

1) a Morse function (its critical points are nondegenerate),
2) smooth on $\mathcal{F}$ (at least a $\mathcal{C}^2$ function),
3) polar at q_d (q_d is a unique minimum), and
4) admissible on $\mathcal{F}$ (uniformly maximal on $\partial\mathcal{F}$).

A general form of navigation functions for the i-th vehicle can be parameterized as [4]:

$$V_i(\mathbf{q}) = \frac{\gamma_i(\mathbf{q})}{\sqrt[k]{\gamma_i^k(\mathbf{q}) + \beta_i(\mathbf{q})}}, \tag{5}$$

where:

- $\gamma_i(\mathbf{q}_i) : \mathcal{F}_i \rightarrow \mathbf{R}_+$ is *the path planning function* which includes the goal and path attraction terms, and reach a unique minimum when the i-th vehicle is at its goal.
- $\beta_i(\mathbf{q}_i) : \mathcal{F}_i \rightarrow [0, 1]$ is the *obstacle function* that fades out when the i-th vehicle collide with other vehicles or static obstacles.
- k is a positive tuning parameter.

In [6], γ_i was designed by adding the distance from the goal to the nominal path d_i weighted by a parameter K_p, i.e.,

$$\gamma_i(\mathbf{q}) = \|\mathbf{q}_i - \mathbf{q}_{d_i}\|^2 + K_p \beta \left(\frac{\|\mathbf{q}_i - \mathbf{q}_{d_i}\|}{r_p} \right) d_i^2, \tag{6}$$

where $d_i = \frac{\|(\mathbf{q}_{o_i} - \mathbf{q}_{d_i}) \times (\mathbf{q}_i - \mathbf{q}_{d_i})\|}{\|\mathbf{q}_{o_i} - \mathbf{q}_{d_i}\|}$ and the function β smoothly transitions from zero to one as defined in (8); in fact, it dims down the path attraction force once the vehicle gets closer than r_p to the goal.

The obstacle function $\beta_i(\mathbf{q})$ is constructed from the product of pairwise functions of obstacles in $\mathcal{N}_i$ and that of the configuration space, in other words, as

$$\beta_i(\mathbf{q}) = \prod_{\mathbf{q}_j \in \mathcal{N}_i} \beta(r_{ij}) \beta(r_{ic}), \tag{7}$$

where $r_{ij} = \frac{(\|\mathbf{q}_j - \mathbf{q}_i\| - \rho_j)}{\delta_j}, r_{ic} = \frac{(\rho_c - \|\mathbf{q}_c - \mathbf{q}_i\|)}{\delta_c}$, ρ_c is a configuration space radius centered at $\mathbf{q}_c$, ρ_j is an obstacle radius centered at $\mathbf{q}_j$, and β is a barrier function used in [1], [6], assuming the form

$$\beta(r_{ij}) = \begin{cases} 0 & r_{ij} < 0, \\ f(r_{ij}) & 0 \leq r_{ij} < 1, \\ 1 & r_{ij} \geq 1; \end{cases} \tag{8}$$

$f(r_{ij})$ is a high order polynomial, shown in Fig. 2, that smoothly transforms $\beta_i(\mathbf{q})$ from being uniformly zero at the collision zone boundary to one at the protected zone boundary. Since $\beta(r_{ij})$ is always one when $\mathbf{q}_i$ is outside the vehicle j's protected zone, we do not include vehicles that are out-of-range in order to compute $\beta_i(\mathbf{q})$. At the

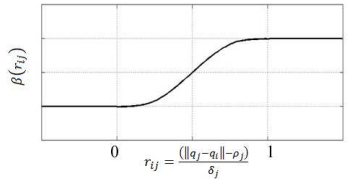

Fig. 2. Sigmoidal shape of the collision function $\beta(r_{ij})$

boundary of $\mathcal{F}_i$, $\beta_i(\mathbf{q}) = 0$ and the potential reaches the

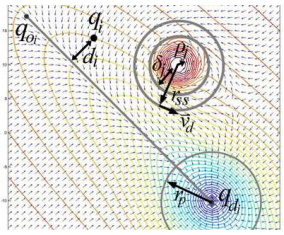

Fig. 3. The gradient vectors across the free configuration space

maximum value of one, and when $\mathbf{q}_i = \mathbf{q}_d$, $\gamma_i(q) = 0$, and the potential reaches its unique minimum. The function is twice differentiable on $\mathcal{F}$ and maps to the unit interval $[0, 1]$. The proof that (5) is a Morse function is shown in [7]. Fig. 3 depicts the corresponding gradient vectors throughout the configuration space.

A. Deconfliction Control

The inner-loop controller of the UAVs to follow the desired velocity will be designed in the form

$$u_i \quad = \quad K(\psi_i^d - \psi_i) + \dot{\psi}_i^d, \tag{9}$$

where K is the control gain, $\psi_i^d = \mathbf{atan}_2\left(v_{y_i}^d, v_{x_i}^d\right)$, where $\mathbf{atan}_2$ is the 4-quadrants arctangent function, and $[v_{x_i}^d; v_{y_i}^d] = \mathbf{v}_i^d(\mathbf{q}) = -\nabla_{\mathbf{q}_i} V_i(\mathbf{q})$. The feed-forward terms $\dot{\psi}_i^d$ is calculated using $[\dot{v}_{x_i}^d; \dot{v}_{y_i}^d] = \dot{\mathbf{v}}_i^d(\mathbf{q}) = -\nabla_{\mathbf{q}} \nabla_{\mathbf{q}_i} V_i(\mathbf{q}) \dot{\mathbf{q}}$, which represents the changes of the potential slope in the $\dot{\mathbf{q}}_i$ direction. This increases the tracking performance once the error has converged to zero.

B. Swirling Effects

Due to the nature of the unicycle model, necessitating control over heading only, the collision avoidance can not be guaranteed by merely following the negative gradient of the navigation function, e.g., if the protected zone is too small compared with the vehicle's speed, the UAV needs to turn very sharp in order to avoid the obstacle. In order to improve the deconfliction performance and help guarantee the collision avoidance under such dynamic limitations, a swirling effect is added to steer the aircraft counterclockwise around the obstacle. The effect grows gradually from the distance for detecting obstacles, r_{ss}, to the maximum value of K_s relative to the original gradient at the boundary of the collision zone. The swirling effect also helps break the symmetry in order to avoid being trapped in saddle points around the obstacles. The adjusted gradient is derived as,

$$\nabla_{\mathbf{q}_i} V_i^{new}(\mathbf{q}) = \nabla_{\mathbf{q}_i} V_i(\mathbf{q}) + K_s \beta_i\left(\tfrac{r_{ss} - \|\mathbf{q}_i - \mathbf{q}_j\|}{r_{ss}}\right) \|\nabla_{\mathbf{q}_i} V_i(\mathbf{q})\| \mathbf{v}_{ss}$$

$$\mathbf{v}_{ss} = \frac{(\mathbf{q}_i - \mathbf{q}_j) \times k_z}{\|\mathbf{q}_i - \mathbf{q}_j\|}, \tag{10}$$

where $\mathbf{q}_i$ and $\mathbf{q}_j$ are the locations of the UAVs and the obstacles, respectively, and k_z is the unit vector in the z-direction. If more than one vehicle is in the range of detection, the superposition of the effects may be used with the barrier function in order to help emphasize the effects from the closer vehicles. Fig. 3 shows the swirling effect of radius r_{ss} around the obstacle.

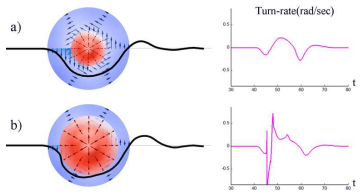

Fig. 4. (a) Avoiding the obstacle without entering protected zone (b) Turn rate increases dramatically when the UAV enters obstacle's protected zone

IV. Collision Avoidance under Turn-Rates Limits

For better tracking performance, the algorithm should generate commands within the limit (1). In this direction, one can examine the spatial derivatives of the gradient vector across the configuration space; since the magnitude of the gradient is not used in our approach, we only consider the change of its direction.

Intuitively the gradient changes at lower rates when the potential gets smoother or when the protected zone is enlarged. However, Fig. 4 shows that for unicycle UAVs, the turn-rate increases dramatically when entering the obstacle's protected zone due to the additional gradient pointing out from the obstacle. This suggests that we should let the swirling effect dominate the collision avoidance or that the vehicle stay in region $\mathcal{Q} = \{\mathbf{q} \,|\, \delta_j < \|\mathbf{q} - \mathbf{q}_j\| < r_{ss}\}$ in order put the turn-rate under the desired limit.

A. The Design Parameters that Affect UAVs Turn-Rates

We now consider the parameters that influence the UAV turn rates under the deconfliction algorithm.

1) Tuning Parameter k:

Proposition 4.1: The parameter k, which adjusts the emphasis between obstacle avoidance and path planning, does not change the direction of the corresponding gradient if the vehicle stays outside the obstacle's protected zone.

Proof: The gradient of the navigation function is

$$\nabla_{\mathbf{q}_i} V(\mathbf{q}) = \frac{k\beta_i(\mathbf{q}) \nabla_{\mathbf{q}_i} \gamma_i(\mathbf{q}) - \gamma_i(\mathbf{q}) \nabla_{\mathbf{q}_i} \beta_i(\mathbf{q})}{k(\gamma_i(\mathbf{q})^k + \beta_i(\mathbf{q}))^{1/k+1}}.$$

If the aircraft stays outside obstacles' protected zones, $\beta(\mathbf{q})$ stays constant at one and $\nabla_{\mathbf{q}_i} \beta_i = \mathbf{0}$. Moreover, the gradient becomes $\nabla_{\mathbf{q}_i} V(\mathbf{q}) = (\gamma_i^k + 1)^{-\frac{k+1}{k}} \nabla_{\mathbf{q}_i} \gamma(\mathbf{q})$. The identity (6) shows that $\nabla_{\mathbf{q}_i} \gamma(\mathbf{q})$ is not a function of k. Therefore the parameter k can only change the magnitude but not the direction of the gradient vector. ■

2) Path Attraction Parameters K_p and r_p: Increasing K_p gives more emphasis on path attraction and leads to higher turn-rate when the vehicle turns to the nominal path toward its goal.

Proposition 4.2: When the UAV (1) with a unity constant speed under the direction of the deconfliction algorithm (4), (5), and (6), turns to the planned-path toward the goal point, the path attraction turn rate is bounded by $\frac{K_p \sqrt{2}}{3\sqrt{3} r_p}$.

3) Swirling Parameters K_s and r_{ss}: By exploring the adjusted gradient (10), we found a *singular point* at the boundary of the swirling zone behind the obstacle where the turn-rate goes unbounded (Fig. 5), i.e., the property of being a $\mathcal{C}^2$-function is not met due to a sudden change of the gradient to the opposite direction caused by the

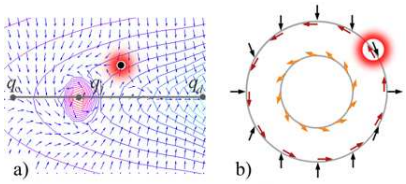

Fig. 5. The singular point at the boundary of the swirling zone

swirling term. An effective approach to avoid this area will be discussed subsequently. Meanwhile, the parameters K_s and r_{ss} also have effects on turn-rates inside the swirling zone. As we increase r_{ss}, the swirling term grows slower resulting in lower turn-rates. On the contrary, the effect is more emphasized when K_s is increased and the aircraft turns at a higher rate.

Proposition 4.3: When a vehicle heads directly toward the obstacle and enters the swirling zone with unit velocity, the turn rate is bounded by mK_s/r_{ss}, where m is the maximum slope induced by the barrier function (8).

Proof: Swirling vectors are added perpendicular to the original gradient in a pattern similar to the barrier function (8), as shown in Fig. 6. Since (8) is normalized to unity, the change in swirling term is scaled by K_s and $1/r_{ss}$. Thus, the adjusted gradient has the rate bounded by mK_s/r_{ss} and the turn rate $\omega \leq \lim_{dt\to 0}\left(\tan^{-1}\left(\frac{mK_s dt}{r_{ss}}\right)/dt\right) = \frac{mK_s}{r_{ss}}$. ■

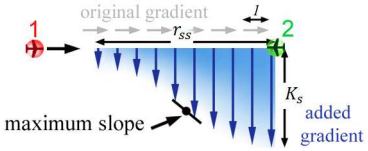

Fig. 6. Swirling parameters

The bound in Proposition 4.3 only applies when the vehicle heads directly toward the obstacle. However, the plot in Fig. 5(b) suggests that the angles between the original gradients and the added swirling gradients do not deviate much from 90^o except in the region near the singular point.

Propositions 4.1, 4.2, and 4.3 help landscape the navigation function (choosing k, K_p, and r_p) and adjusting swirling effects (choosing K_s and r_{ss}) such that the desired heading command stays within the turn-rate limits. Since k does not affect the turn-rate, we pick k such that the region far from the boundary and the goal has potential value around 0.5.

B. Swirling Effects Reduction

Proposition 4.3 suggests that the turn-rate is reduced by increasing the radius r_{ss}. However, this tends to swing the vehicle overshoot to the high turn-rate zone even more (Fig. 7c). This overshoot reduces the aircraft tracking performance and the high turn-rate command results in some delay for the aircraft to come back to the nominal path.

In order to address this issue, we reduce the swirling effect once two vehicles are out of the course of collision. Specifically, we employ the concept of "collision cone" and relative velocity as used in [2], [8]. A collision cone is defined by the region inside the rays drawn from the vehicle to the obstacle collision zone. The *safety angle* measures how far the two vehicles are away from the course of collision.

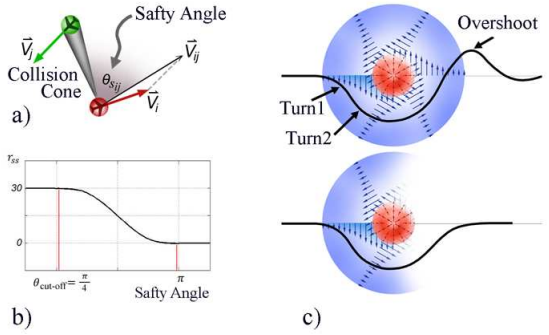

Fig. 7. (a) The collision cone and safety angle, (b) The plot of swirling radius adjusted by safety angle, (c) The overshoot disappears after swirling effect is dimmed down

Definition 4.1: A safety angle for vehicle i from vehicle j, $\theta_{s_{ij}}$, is the angle between the relative velocity $\mathbf{v}_{ij} = \mathbf{v}_i - \mathbf{v}_j$ and the collision cone drawn from vehicle i to vehicle j's collision zone (Fig. 7a).

Our approach is to reduce swirling radius according to the safety angle: from r_{ss} at the cut-off angle to zero when the safety angle equals π, using barrier function pattern (Fig. 7b):

$$r_{ss}^{adjusted}(\theta_s) = \begin{cases} r_{ss} & \theta_s \leq \theta_{cutoff}, \\ r_{ss}\beta\left(\frac{\pi-\theta_s}{\pi-\theta_{cutoff}}\right) & \theta_s > \theta_{cutoff}. \end{cases} \quad (11)$$

For a smooth trajectory, the cut-off angle is chosen to be around $\frac{\pi}{4}$. Fig. 7c shows that this concept prevents the vehicle from overshooting into the high turn-rate zone.

C. Swirling Effect and Guaranteed Deconfliction

In this section, we explore the guaranteed convergence of the algorithm to collision-free state under the navigation law dictated by the swirling effect. It is proven that when the vehicles get within the "radar range" of each other (region $\mathcal{Q}$) and the algorithm is applied, their protected zones will not intersect at all future times until they get out of the region $\mathcal{Q}$. In order to simplify the proof, we adopt the following assumptions:

Assumption 4.1: Two vehicles start from the distance that they can detect each other r_{ss} and the conflict is resolved before the next vehicle comes in.

Assumption 4.2: The vehicles are far from destinations and the gradients are primary due to the swirling effect and (10) becomes $\nabla V_i = \frac{(\mathbf{q}_i - \mathbf{q}_j)\times k_z}{\|\mathbf{q}_i - \mathbf{q}_j\|}$. The desired heading is $\psi_i^d = \mathbf{atan}_2(x_i - x_j, y_j - y_i)$, and the feed-forward term is

$$\begin{aligned}\dot{\psi}_i^d &= \frac{-(y_j-y_i)^2}{(x_j-x_i)^2+(y_j-y_i)^2}\left[\frac{(y_j-y_i)(\dot{x}_j-\dot{x}_i)-(x_j-x_i)(\dot{y}_j-\dot{y}_i)}{(y_j-y_i)^2}\right] \\ &= -U\left[\frac{\cos(\psi_j^d-\psi_j)+\cos(\psi_i^d-\psi_i)}{\sqrt{(x_j-x_i)^2+(y_j-y_i)^2}}\right]. \end{aligned} \quad (12)$$

Now let $\bar{x} = x_1 - x_2$, $\bar{y} = y_1 - y_2$ and the system of two vehicles under the swirling effects is represented as:

$$\begin{aligned} \dot{\bar{x}} &= U(\cos\psi_1 - \cos\psi_2) && , \bar{x}(0) = -r_{ss} \\ \dot{\bar{y}} &= U(\sin\psi_1 - \sin\psi_1) && , \bar{y}(0) = 0 \\ \dot{\psi}_1 &= K(\psi_1^d - \psi_1) + U\left(\frac{\cos(\psi_2^d-\psi_2)+\cos(\psi_1^d-\psi_1)}{\sqrt{\bar{x}^2+\bar{y}^2}}\right) && , \psi_1(0) = \psi_{1_0} \\ \dot{\psi}_2 &= K(\psi_2^d - \psi_2) + U\left(\frac{\cos(\psi_2^d-\psi_2)+\cos(\psi_1^d-\psi_1)}{\sqrt{\bar{x}^2+\bar{y}^2}}\right) && , \psi_2(0) = \psi_{2_0} \\ & , \psi_1^d = \mathbf{atan}_2(\bar{x}, -\bar{y}), \psi_2^d = \mathbf{atan}_2(-\bar{x}, \bar{y}) \end{aligned} \quad (13)$$

where ψ_{1_0} and ψ_{2_0} are the initial headings when they enter the swirling zone within distance r_{ss} apart. Fig. 8 shows the

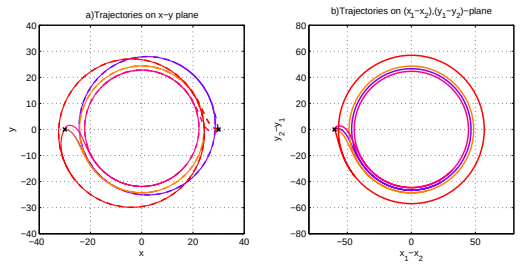

Fig. 8. (a) Trajectories of 2 UAVs under the swirling effects with 4 different initial headings (b) Trajectories on $\bar{x}, \bar{y}$-plane

trajectories of two vehicles according to (13) with different of initial headings. Swirling effects drive the two vehicles to converge into a circle and stay on the opposite side, heading in opposite directions. We note that different pairs of initial headings result in convergence to different limit cycles.

Now we use LaSalle's Invariance Principle to prove that two vehicles under the swirling effect converge to a limit cycle whose diameter is the minimum distance between the two vehicles. The limit cycle is written as an invariant set

$$\mathcal{M} = \{(\bar{x},\bar{y},\psi_1,\psi_2) \in \mathbf{R}^4; \bar{x}^2+\bar{y}^2 = R^2, \\ \psi_1 = \mathbf{atan}_2(\bar{x},-\bar{y}), \psi_2 = \mathbf{atan}_2(-\bar{x},\bar{y})\}, \quad (14)$$

where R is a radius of the limit cycle.

Theorem 4.1: The two vehicles under the swirling effect in (13) converge to the limit cycle (14) and get no closer than $2R$ when they start from r_{ss} apart with initial headings ψ_{1_0} and ψ_{2_0}, respectively.

Proof: First, we show that $\mathcal{M}$ is invariant by

$$\begin{aligned}
&\tfrac{d}{dt}(\bar{x}^2+\bar{y}^2-R^2) = 2(\bar{x}\dot{\bar{x}}+\bar{y}\dot{\bar{y}}) \\
&\quad = 4UR(\sin\psi_1^d(\cos\psi_1-\cos\psi_2)+\cos\psi_1^d(\sin\psi_1-\sin\psi_2)) \\
&\quad = 4UR(\sin(\psi_1^d-\psi_1)+\sin(\psi_2^d-\psi_2)) = 0 \\
&\tfrac{d}{dt}\left(\mathbf{atan}_2(\bar{x},-\bar{y})-\psi_1\right) = \tfrac{d}{dt}\left(\mathbf{atan}_2(\bar{x},-\bar{y})\right)-\dot{\psi}_1 \\
&\quad = -\left[K\left(\mathbf{atan}_2(\bar{x},-\bar{y})-\psi_1\right)\right] \\
&\quad = 0 = \tfrac{d}{dt}\left(\mathbf{atan}_2(-\bar{x},\bar{y})-\psi_2\right). \qquad (15)
\end{aligned}$$

If $(\bar{x}(0),\bar{y}(0),\psi_1(0),\psi_2(0)) \in \mathcal{M}$, then $(\bar{x}(t),\bar{y}(t),\psi_1(t),\psi_2(t)) \in \mathcal{M}, t \geq 0$. The motion on $\mathcal{M}$ is characterized by $\dot{\psi}_1 = \dot{\psi}_2 = U/R$ which shows that $\mathcal{M}$ is a limit cycle for (13) where the state vector moves counterclockwise.

In order verify that $\mathcal{M}$ is attractive, define the function $V : \mathbf{R}^4 \to \mathbf{R}$, representing how far the system is from the limit cycle. Let

$$V(\bar{x},\bar{y},\psi_1,\psi_2) = (\bar{x}^2+\bar{y}^2-R^2)^2+(\psi_1^d-\psi_1)^2+(\psi_2^d-\psi_2)^2,$$

and observe that

$$\begin{aligned}
\dot{V}(\bar{x},\bar{y},\psi_1,\psi_2) &= 4(\bar{x}^2+\bar{y}^2-R^2)(\bar{x}\dot{\bar{x}}+\bar{y}\dot{\bar{y}}) \\
&\quad +2(\psi_1^d-\psi_1)(\dot{\psi}_1^d-\dot{\psi}_1)+2(\psi_2^d-\psi_2)(\dot{\psi}_2^d-\dot{\psi}_2).
\end{aligned}$$

It is easy to see that $\dot{V} = 0$ on $\mathcal{M}$. We now examine the case when the vehicles start outside the limit cycle and let

$$\begin{aligned}
&\dot{V}_1 = 4(\bar{x}^2+\bar{y}^2-R^2)(\bar{x}\dot{\bar{x}}+\bar{y}\dot{\bar{y}}) \\
&= 4U(\bar{x}^2+\bar{y}^2-R^2)\sqrt{\bar{x}^2+\bar{y}^2}(\sin(\psi_1^d-\psi_1)+\sin(\psi_2^d-\psi_2)).
\end{aligned}$$

As ψ_{1_0}, ψ_{2_0} face each other (or, without loss of generality, $\psi_{1_0} \in (-\frac{\pi}{2},\frac{\pi}{2}), \psi_{2_0} \in (\frac{\pi}{2},\frac{3\pi}{2})$), swirling effects will direct the planes to go around each other and converge to $\mathcal{M}$. In this case, both UAVs converge to $\mathcal{M}$ from outside and that $\bar{x}^2+\bar{y}^2 > R^2$. Fig. 9 shows that $-\pi < \psi_1^d-\psi_1 < 0$, $-\pi < \psi_2^d-\psi_2 < 0$ for all times before the trajectories approach $\mathcal{M}$ and $\sin(\psi_1^d-\psi_1) < 0, \sin(\psi_2^d-\psi_2) < 0$. Hence, $\dot{V}_1 < 0$. Since that the swirling effect is not applied to other sets of initial conditions due to the large safety angle, the proof of validity of the inequality $\dot{V}_1 < 0$ for those scenarios are not shown here. Now let $\dot{V}_2 = -2K[(\psi_1^d-\psi_1)^2+(\psi_2^d-\psi_2)^2] \leq 0$, and hence $\dot{V} < 0$ anywhere outside $\mathcal{M}$. For $\beta > 0$, let

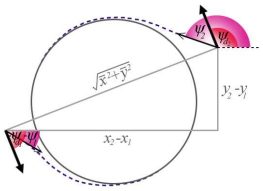

Fig. 9. The headings and desired heading of 2 vehicles under swirling effects when they in the course of collision

$$\mathcal{D}_c = \{(\bar{x},\bar{y},\psi_1,\psi_2) \in \mathbf{R}^4; V(\bar{x},\bar{y},\psi_1,\psi_2) \leq \beta\} \quad (16)$$

and $\dot{V} \leq 0$ everywhere in $\mathcal{D}_c$. Define $\mathcal{R} = \{(\bar{x},\bar{y},\psi_1,\psi_2) \in \mathbf{R}^4; \dot{V}(\bar{x},\bar{y},\psi_1,\psi_2) = 0\}$. The largest invariant set in $\mathcal{R}$ is $\mathcal{M}$. It now follows from LaSalle's Invariance that all system trajectories starting in $\mathcal{D}_c$ converge to $\mathcal{M}$, or when the two vehicles evolve under the swirling effect in (13) with $(\bar{x}(0),\bar{y}(0),\psi_1(0),\psi_2(0)) = (-r_{ss},0,\psi_{1_0},\psi_{2_0}) \subseteq \mathcal{D}_c$, then $(\bar{x}(t),\bar{y}(t),\psi_1(t),\psi_2(t)) \to \mathcal{M}$ as $t \to \infty$ ■

We note that when the swirling effect is reduced by the safety angle method discussed above, the vehicles stay in the limit cycle only until they face away from each other and continue toward their respective original paths. It is also noteworthy to point out the relationship between the algorithm parameters and the minimum distance between the vehicles. In fact, the distance between two vehicles in (13) is $d = \sqrt{\bar{x}^2+\bar{y}^2}$ and its time derivative is

$$\dot{d} = \frac{1}{d}(\bar{x}\dot{\bar{x}}+\bar{y}\dot{\bar{y}}) = U(\sin(\psi_1^d-\psi_1)+\sin(\psi_2^d-\psi_2)).$$

For $i = 1, 2$, let $\alpha_i = \psi_{d_i}-\psi_i$; its time derivative is then

$$\dot{\alpha}_i = \dot{\psi}_{d_i}-[K(\psi_i^d-\psi_i)+\dot{\psi}_i^d] = -K\alpha_i.$$

The distance between two vehicles under the swirling effect in (13) is thus governed by: (a) $\dot{d} = U[\sin\alpha_1+\sin\alpha_2]$ when $d(0) = r_{ss}$, (b) $\dot{\alpha}_1 = -K\alpha_1$ when $\alpha_1(0) = \alpha_{1_0} \in [-\pi,0]$, and (c) $\dot{\alpha}_2 = -K\alpha_2$ when $\alpha_2(0) = \alpha_{2_0} \in [-\pi,0]$.

Theorem 4.2: The system of two vehicles under swirling effects (13) attains the minimum distance of $d_{\min} = r_{ss} - \frac{U}{K}[\mathrm{Si}(|\alpha_{1_0}|) + \mathrm{Si}(|\alpha_{2_0}|)]$, where $\mathrm{Si}(x)$ is a sine integral function defined in [12].

Proof: From the above discussion, we have $\alpha_1(t) = \alpha_{1_0}e^{-Kt}$ and $\alpha_2(t) = \alpha_{2_0}e^{-Kt}$ and the distance between two vehicles is

$$\begin{aligned}
d(t) &= d(0)+\int_0^t U[\sin(\alpha_{1_0}e^{-Kt})+\sin(\alpha_{2_0}e^{-Kt})]\,dt \\
&= r_{ss}-\frac{U}{K}\left[\int_{\alpha_{1_0}}^{\alpha_1(t)}\frac{\sin\alpha_1}{\alpha_1}\,d\alpha_1+\int_{\alpha_{2_0}}^{\alpha_2(t)}\frac{\sin\alpha_2}{\alpha_2}\,d\alpha_2\right] \\
&= r_{ss}-\frac{U}{K}[\mathrm{Si}(|\alpha_{1_0}|)-\mathrm{Si}(|\alpha_1(t)|)+\mathrm{Si}(|\alpha_{2_0}|)-\mathrm{Si}(|\alpha_2(t)|)]
\end{aligned}$$

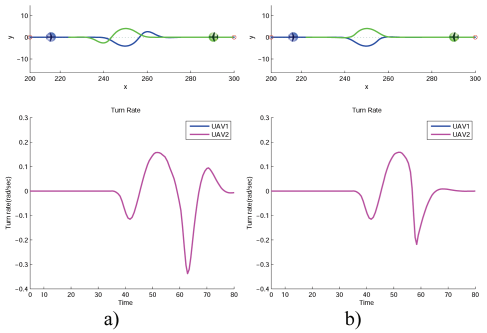

a) b)

Fig. 10. Trajectory and turn rate of head-on case with $r_{ss} = 30$: (a) Swirling effect causes overshoots, (b) The overshoot disappears by safety angle method

and the minimum distance is thereby

$$d_{\min} = \lim_{t\to\infty} d(t) = r_{ss} - \frac{U}{K}[\text{Si}(|\alpha_{1_0}|) + \text{Si}(|\alpha_{2_0}|)]. \quad (17)$$

The worst initial headings that lead to the shortest minimum distance occur when Si-function reach its maximum at $\alpha_{1_0} = \alpha_{2_0} = -\pi$ (This is not the case when the safety angle method is applied). The minimum distance thus becomes $d_{\min} = r_{ss} - \frac{2U}{K}[\text{Si}(\pi)] \approx r_{ss} - \frac{3.704U}{K}$. ■

According to the initial headings, we use (17) to pick a cruising speed U, control gain K, and the detection range r_{ss} such that $d_{\min}$ is greater than vehicles' protected zone. This formula is made under Assumption 4.2 which means that the algorithm rotate the vehicles with lower rates– in this case– a safety factor should be embedded in the algorithm.

For the case when the other vehicles come into conflict at the same time or before the swirling effect between the two vehicles terminates, the superposition of the effects from each vehicles can be used with the barrier function in order to help emphasizing the effects from the closer vehicles. The convergence of such an extended deconfliction scenario, however, needs to be studied further and is not addressed in the present paper.

V. Simulation Results

Fig. 10 compares the simulation results for the head-on case and when the turn-rate limit is set at 0.5 rad/sec. The parameters are chosen based on section IV in order to meet the turn-rate constraint and to guarantee the minimum distance between vehicles: $k = 0.2, r_p = 20, K_p = 20, K_s = 2$, and $r_{ss} = 30$. Other parameters are set as follow: $\delta_j = \delta_c = 5, \rho_j = 0, \rho_c = 2000$ and the control gain $K = 0.6$. After we reduce the swirling effect with $\theta_{cutoff} = \frac{3\pi}{8}$, the trajectories no longer have an overshoot and the turn rates are reduced to 0.2 rad/sec. Fig. 11 shows another example for the deconfliction maneuver when five UAVs accidently attempt to fly through the same coordinate.

VI. Conclusion

In this paper, a deconfliction algorithm for unicycle UAVs based on the navigation function has been developed. The performance of the algorithm is inspected with respect to key parameters and the mission specific restrictions such as turn-rate limits and constant velocity. In this avenue, the proposed navigation function has been landscaped by adjusting the swirling effect such that the vehicles operate within their turn-rate limitations. Finally, the convergence analysis of the algorithm is performed based on the assumption that the swirling effect is dominant during the deconfliction maneuver between a pair of UAVs. There are a few possible extensions of this work. First, velocity information of the sensed obstacles can be considered in the potential function construction to improve the performance. The second extension involves allowing the UAV speed to vary between its stall and maximum speed, as well as making use of the magnitude of the gradients of the navigation function. Third, the convergence analysis when three or more vehicles come into the range of detection of each other simultaneously should be formalized.

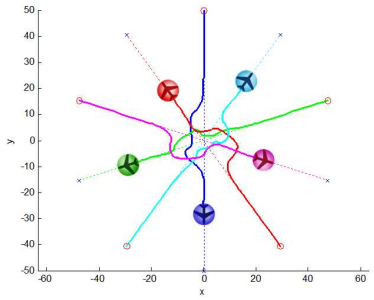

Fig. 11. Simulation trajectories when 5 vehicles fly through the same point

References

[1] M. De Gennaro and A. Jadbabaie Formation control for a cooperative multi-agent system using decentralized navigation functions, *American Control Conference*, June, 2006.

[2] E. Frazzoli, Z. Mao, J. Oh, and E. Feron Resolution of conflicts involving many aircraft via semidefinite programming, *Journal of Guidance, Control, and Dynamics*, (24) 1: 79-86, 2001.

[3] O. Brock and O. Khatib. High-Speed navigation using the global dynamic window approach, *Proceedings of IEEE International Conference on Robotics and Automation*, Detroit, MI, pp. 341-346, 1999.

[4] E. Rimon and D. Koditschek. Exact robot navigation using artificial potential functions, *IEEE Transactions on Robotics and Automation*, (8) 5: 501-518, 1992.

[5] E. Rimon and D. Koditschek. Robot navigation function on manifold with boundary, *Advanced in Applied Mathematics*, (11) 4: 412-442, 1990.

[6] A. Rahmani, K. Kosuge, T. Tsukamaki, and M. Mesbahi. Multiple UAV Deconfliction via Navigation Functions, *American Control Conference*, 2007.

[7] P. Panyakeow and M. Mesbahi. On Deconfliction Algorithms for Unicycle Model of Unmanned Aerial Vehicles, University of Washington, 2009.

[8] E. Lalish, K. Morgansen, and T. Tsukamaki. Decentralized reactive collision avoidance for multiple unicycle-type vehicles, *American Control Conference*, 2008.

[9] C. Carbone, U. Ciniglio, F. Corraro, and L. Luongo. A novel 3D geometric algorithm for aircraft autonomous collision avoidance, *IEEE Conference of Decision and Control*, 2006.

[10] J. Kuchar and L. Yang. A review of conflict detection and resolution modeling methods, *IEEE Transactions on intelligent transportation system*, 2000.

[11] I. Hwang and C. Tomlin. Protocol-based conflict resolution for air traffic control, Standford University, Tech.Rep SUDAAR-762, 2002.

[12] M. Abramowitz and I. Stegun. Handbook of mathematical functions with formulas, graphs, and mathematical tables, Dover, 1972.

[13] D. Dimarogonas and K. Kyriakopoulos. Decentralized stabilization and collision avoidance of multiple air vehicles with limited sensing capabilities, *American Control Conference*, 2005.

[14] D. Dimarogonas and K. Kyriakopoulos. Decentralized motion control of multiple agents with double integrator dynamics, *IFAC*, 2005.